Effect of Cross-Linking Properties on the Vibrational Dynamics of Cyclodextrins-Based Polymers: An Experimental-Numerical Study

ARTICLE *in* THE JOURNAL OF PHYSICAL CHEMISTRY B · JUNE 2012

Impact Factor: 3.3 · DOI: 10.1021/jp303006a · Source: PubMed

7 AUTHORS, INCLUDING:

Andrea Mele
Politecnico di Milano
208 PUBLICATIONS **2,716** CITATIONS
SEE PROFILE

Barbara Rossi
Elettra, Sincrotrone Trieste S.C.p.A.
63 PUBLICATIONS **430** CITATIONS
SEE PROFILE

Francesco Trotta
Università degli Studi di Torino
150 PUBLICATIONS **2,501** CITATIONS
SEE PROFILE

THE JOURNAL OF PHYSICAL CHEMISTRY B

Article

pubs.acs.org/JPCB

Effect of Cross-Linking Properties on the Vibrational Dynamics of Cyclodextrins-Based Polymers: An Experimental–Numerical Study

Franca Castiglione,[†] Vincenza Crupi,[‡] Domenico Majolino,[‡] Andrea Mele,[†] Barbara Rossi,*[,§,∥] Francesco Trotta,[⊥] and Valentina Venuti[‡]

[†]Department of Chemistry, Materials and Chemical Engineering "G. Natta", Politecnico di Milano, Via Mancinelli 7, 20131 Milano, Italy

[‡]Dipartimento di Fisica, Università di Messina and CNISM UdR Messina, Viale Ferdinando Stagno D'Alcontres 31, 98166 Messina, Italy

[§]Dipartimento di Informatica, Università di Verona, Strada le Grazie 15, 37134 Verona, Italy

[∥]Dipartimento di Fisica, Università di Trento, Via Sommarive 14, 38123 Povo, Trento, Italy

[⊥]Dipartimento di Chimica, Università di Torino, Via Pietro Giuria 7, 10125 Torino, Italy

ABSTRACT: The vibrational dynamics of cyclodextrin nanosponges (CDNS), a new class of nanostructured soft materials synthesized via cross-linking reaction of natural cyclic oligosaccharide β-cyclodextrin (β-CD) with suitable organic reagents, is investigated by means of the combined use of Raman and infrared spectroscopy, supported by numerical simulations. The vibrational spectra of the polymers show significant changes in the frequency ranges 3000–3700 and 1500–1800 cm^{-1} correlated to the relative amount of cross-linker with respect to monomeric CD. By using band deconvolution and best-fit procedure of the experimental data and quantum chemical computations, a correlation between such changes and the degree of cross-linking of the polymeric network is proposed. This experimental–numerical approach, here applied to a model class of nanoporous polymeric systems, appears to be of general application for the study of polymeric matrixes of interest for biolife applications.

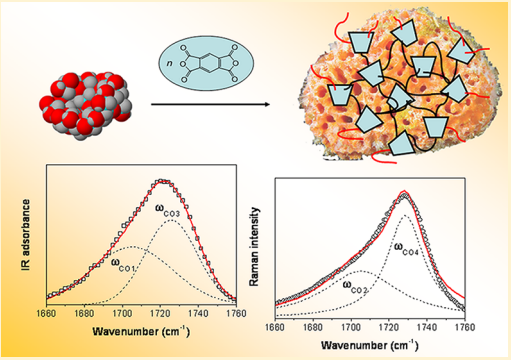

INTRODUCTION

Cyclodextrin nanosponges (CDNS) are a new class of cross-linked, nanoporous polymers obtained by reaction of cyclodextrins (CDs) with a suitable polyfunctional cross-linking agent, such as pyromellitic anhydryde or carbonyldiimidazole.[1,2] Cyclodextrins are cyclic oligomers of amilose made of 6, 7, or 8 glucopyranose units linked together in a macrocycle by $\alpha(1 \rightarrow 4)$ glycosidic linkage (α-, β-, and γ-cyclodextrin). When treated with an activated derivative of di- or polycarboxylic acid, CDs polymerize in a three-dimensional network where the CD units are connected through ester functional groups with the cross-linker. The main feature of the material thus obtained is the simultaneous presence of lyphophilic cavities and hydrophilic channels, which can be used to encapsulate, carry, and/or release a large variety of substances.[3−8] Moreover, the use of different cross-linking agents provides a useful modulation of physicochemical properties of the final material. For these reasons, CDNS have been exploited in a variety of fields, including biocatalysis, agriculture, environmental control, and pharmaceutical applications.[9−12] In particular, they have been proven to form inclusion and non-inclusion complexes with different lipophilic and hydrophilic drugs and to facilitate their gradual release over extended times, increasing the bioavailability at the target site.[6,7]

CDNS are generally insoluble in water and in common organic solvents, even if some classes of them exhibit intriguing properties of swelling in the presence of aqueous solutions, similarly to hydrogels. Their swelling ability and hydrophilicity/hydrophobicity properties can be modulated by properly choosing the cross-linking agent and varying the molar ratio between CD and cross-linker during the polymerization.

The physicochemical properties of β-cyclodextrin-based nanosponges (β-CDNS) have been principally investigated by differential scanning calorimetry (DSC)[3] and X-ray powder diffraction techniques;[13] data revealed a prevalently amorphous structure and a high thermal stability, up to ~320 °C. Recently, high resolution magic angle spinning nuclear magnetic resonance (HRMAS-NMR) measurements on hydrated β-CDNS evidenced the presence, inside the polymeric network, of free and bound water molecules characterized by different diffusion coefficients.[13] Nevertheless, we are still far from a complete structural and dynamical characterization at molecular level of these innovative materials. In particular, (i) it is still unknown how CD molecules are assembled in the polymeric

Received: March 29, 2012
Revised: May 24, 2012
Published: June 13, 2012

network of nanosponges, (ii) few experimental investigations aimed at working out any long-range order motif within the CDNS frame have been reported so far, (iii) quantitative data on the distribution of the pores size are still missing, and, finally, (iv) it is not yet clear how the type of cross-linker and its relative amount with respect to CD used during the synthesis of polymers can affect the degree of cross-linking of the final product.

More specifically, the latter question is of fundamental importance in view of the possibility to control and predict the entrapment and transport properties inside the CDNS polymeric matrix and hence for developing and synthesizing nanosponges with physicochemical properties specifically tunable to different needs. This occurrence becomes of crucial relevance, for example, for drug-delivery applications, where the delivery kinetics of drugs could be designed according to the tailored release profile by tuning cross-linking density of the carrier matrix.

The present investigation is performed on a specific class of β-CDNS obtained by reacting β-CD with pyromellitic dianhydride (PMA) in suitable CD/PMA molar ratios, with the aim to better clarify the role played by this parameter on the degree of cross-linking of the polymeric network.

For this purpose, a detailed study of the spectral properties of hydroxyl O−H and carbonyl C═O groups vibrational bands observed in the spectrum of different PMA−nanosponges has been carried out, by using FT-IR spectroscopy in attenuated total reflectance geometry (FTIR-ATR) and Raman spectroscopy, interpreting the main revealed features in terms of cross-linking density of the system. The analysis, quantitatively performed thanks to a best-fit procedure,[14] is supported by quantum chemical computations, which allowed us to unambiguously assign the experimental bands to specific chemical group vibrations. Moreover, the effect of temperature and of the CD/PMA molar ratio on the different H-bonded environments contributing to the high frequency vibrational dynamics of the nanosponges has been clarified.

EXPERIMENTAL METHODS

Synthesis of β-CDNS. In order to obtain β-CDPMA1n nanosponges, the reactions of polymerization between β-CD and cross-linking agent PMA, at β-CD/PMA molar ratios of 1:n (with n = 2, 2.5, 4, 6, 8, and 10) were conducted dissolving the reagents in dimethyl sulfoxide (DMSO) containing triethylamine and allowed to react at room temperature for 3 h. Once the reaction was over, the solid obtained was ground in a mortar and Soxhlet extracted with acetone for 8 h.

FTIR-ATR Measurements. FTIR-ATR measurements were performed, in the temperature range extending from 250 to 310 K, using a Bomem DA8 Fourier transform spectrometer, operating with a Globar source, in combination with a KBr beamsplitter, a DTGS/KBr detector. Spectra were collected in the 600−3700 cm^{-1} wavenumber range. The powders were contained in Golden Gate diamond ATR system, just based on the ATR technique.[15] An ATR setup exhibits various advantages with respect to an ordinary absorption setup. It is nondestructive, it requires only micrograms of sample, and it is at the origin of spectra displaying a very good signal-to-noise ratio, being in particular easy to avoid saturation of bands. In addition, a chemical analysis can be performed directly on ATR spectra, avoiding implementation of elaborated calculations of optical constants.[16,17]

The spectra were recorded in dry atmosphere, in order to avoid dirty contributions, with a resolution of 2 cm^{-1}, automatically adding 100 repetitive scans in order to obtain a good signal-to-noise ratio and high reproducibility. All the IR spectra were normalized for taking into account the effective number of absorbers.

No mathematical correction (e.g., smoothing) was done, and spectroscopic manipulation such as baseline adjustment and normalization were performed using the Spectracalc software package GRAMS (Galactic Industries, Salem, NH, USA). For the O−H stretching region, second derivative computations have been used for evaluating the wavenumbers of the maxima of the different sub-bands. Multiple curve fitting into Voigt profiles were then applied to the experimental profiles based on these wavenumber values, by using the routine provided in the PeakFit 4.0 software package. The statistical parameters defined in the software manual were used as a guide to best-fit and allowed to vary upon iteration until converging solution is reached. The best-fit is characterized by $r^2 \approx 0.9999$ for all the investigated systems.

Raman Measurements. Raman spectra were recorded on dried samples deposited on a glass slide, in air, at room temperature, by means of a microprobe setup (Horiba-Jobin-Yvon, LabRam Aramis) consisting of a He−Ne laser, a narrow-band edge filter, a 46 cm focal length spectrograph using a 1800 grooves/mm grating and a charge-coupled device (CCD) detector. Exciting radiation at 632.8 nm was focused onto the sample surface with a spot size of about 1 μm^2 through a 100× objective with NA = 0.9. To avoid unwanted laser-induced transformations, neutral filters of different optical densities were used, whenever necessary. Spectra were collected in the wavenumber range 100−3700 cm^{-1}. The resolution was about 0.35 cm^{-1}/pixel.

Computational Methods. The molecular model of 1,2,4,5-tetracarboxybenzoic acid dimethyl ester (Figure 5) was built from scratch by using PCMODEL 8.0 package (Serena Software, Bloomington, IN, USA) and allowed to fully relax in the MMX force field.[18] The MMX energy minimized geometry was in turn used as the starting structure for ab initio quantum chemical computations carried out with the Gaussian03 program suite[19] using unrestricted density functional theory (DFT).[20] The nonlocal B3LYP functional hybrid method was employed.[21] The standard 6-31G basis set[22] was used for the geometry optimization and vibrational energy analysis. For the plot of the theoretical infrared and Raman spectra, a Lorentzian line shape with a line width of 4 cm^{-1} was used; computed IR intensities and Raman activities are expressed in arbitrary units.

RESULTS AND DISCUSSION

The combined use of Raman and infrared spectroscopy can provide complementary information on the vibrational dynamics of a molecular system: in fact, although some vibrations may be active in both Raman and IR spectra, the corresponding vibrational bands can appear more or less intense depending on the spectroscopic technique that is used.

The in-depth analysis of the vibrational dynamics of nanosponges in the wavenumber region between 3000 and 3700 cm^{-1} gives important information on the intermolecular hydrogen bond network of the system. Indeed, different vibrational components contributing to the total O−H stretching band[23−28] can be recognized in this spectral range. The center-frequency and IR intensity of the bands are sensitive

dx.doi.org/10.1021/jp303006a | J. Phys. Chem. B 2012, 116, 7952−7958

to the change of the bond strength and the relative populations of differently H-bonded molecules, respectively.

For the analysis of the experimental FTIR-ATR spectra, we followed a well-established approach, already successfully applied to a variety of similar systems,[26−28] based on band deconvolution and curve fitting. According to this model, the O−H stretching profile can be well reproduced by using five spectral contributions assigned to vibrations involving the OH groups of interstitial and intracavity water molecules and the primary and secondary OH groups of cyclodextrin.[29,30] We remark that, in the case of PMA−nanosponges, the OH groups present in the PMA molecule give additional contributions overlapped with those arising from the CD units and that the separation of these spectral components can become not meaningful. For this reason, we decided to apply the approach described above only to β-CDPMA nanosponges obtained by using the lowest β-CD/PMA molar ratio, i.e., 1:2 and 1:2.5. In such cases, we estimated that the contribution of PMA to the whole absorbance is 30% and 36%, respectively. For the higher molar ratios, only a qualitative description was performed.

In order to avoid any overintepretation of the data due to the well-known difficulty of uniquely fitting IR band profiles,[31,32] we evaluated the minima in the second derivative profile of the measured spectra as a first indication of the peak wavenumbers of the corresponding components of the analyzed band (data are not reported). The diagram of the second derivative clearly shows five subminima centered at $\omega_1 \approx 3100$ cm^{-1}, $\omega_2 \approx 3190$ cm^{-1}, $\omega_3 \approx 3270$ cm^{-1}, $\omega_4 \approx 3360$ cm^{-1}, and $\omega_5 \approx 3520$ cm^{-1}. This finding supports the use of five sub-bands, peaked at almost the same center frequencies, for a satisfactory reproduction of the O−H spectral profile. These sub-bands are assigned, in the order, to vibrations of water molecules retained in the interstices among different CD molecules and linked, via H-bond, to the macrocycle of CD (ω_1 and ω_3), water molecules present inside the CD cavity (ω_5), and to stretching vibrations of secondary (ω_2) and primary (ω_4) OH groups of CD.

Figure 1 shows the five spectral components obtained by using the fit procedure for β-CDPMA12 spectra acquired at T = 250, 290, and 310 K; the corresponding main fit parameters, i.e., peak wavenumber (ω_i, cm^{-1}) and percentage intensity (I_i, %) are reported in Table 1.

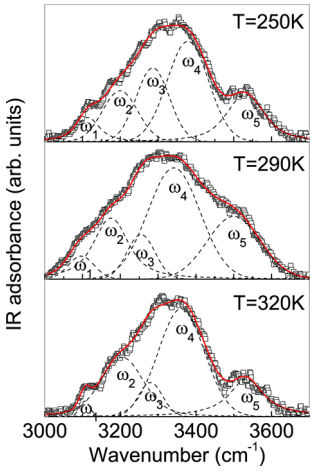

Figure 1. Experimental FTIR-ATR spectra (empty squares) in the OH stretching region for β-CDPMA12 nanosponge, acquired at different temperatures T, together with the best-fit (continuous line) and the deconvolution components (dashed lines).

The peak wavenumbers ω_i (i = 1, 2, 3, 4, and 5) are strictly related to the strength of the corresponding H-bonds as well as to the variations of the average O···O distances in the H-bond network,[24−26] i.e., the more high-shifted the peak frequencies, the more reduced the cooperativity of the H-bonds. For each sub-band, the largest observed frequency shift is less than 20 cm^{-1}, so we are not able to unequivocally assign a maximum, and hence, we can retain this parameter as constant.

The percentage intensities I_i (i = 1, 2, 3, 4, and 5) of the different spectral contributions are representative of the populations of the particular species assigned to each component; in Figure 2, an overall view of their temperature evolution is reported for the β-CDPMA12 sample.

As general trend, the increasing of temperature seems to induce, in the explored T range, destructuring effects on the hydrogen-bonding scheme by disrupting the network of intramolecular and water−CD hydrogen bonds. This is consistent with the observed decrease of the population of interstitial H_2O molecules (described by I_1 and I_3) and increase of the population of secondary and primary OH groups (I_2 and I_4), while the contribution of intracavity H_2O molecules remains essentially unchanged.

More interesting conclusions are achieved by comparing, at a given temperature, the FTIR-ATR spectra as a function of the β-CD/PMA molar ratio (see Table 1). The results from the curve fitting procedure for β-CDPMA at 1:2 and 1:2.5 molar ratios, respectively, are shown in Figure 3a and 3b (data acquired at T = 300 K). The data of Table 1 indicate that increasing the cross-linker amount with respect to CD induces an overall high-frequency shift of the O−H stretching band. This trend is consistent with a progressive disruption of the hydrogen bond networks involving the OH groups of the polymer.

This finding can be further supported by the observed tendency of the C═O stretching band, falling at about 1722 cm^{-1} in the FTIR-ATR spectra of nanosponges (see inset in Figure 3a), to shift to higher values with increasing n, which is in turn ascribed to a strengthening of the double bond in the corresponding carbonyl groups due to the establishment of weaker forces.

The variations of the relative intensities of the five sub-bands of the OH stretching region as a function of the molar ratio n are reported in Figure 3c. The population I_4 (open circles, Figure 3c), corresponding to the primary OH groups of the native cyclodextrin, that are expected to be the most involved in the polymerization process,[14] shows a marked decrease with increasing molar ratio n. The decrease intensity is significantly dependent on the type of cross-linking agent used in the polymerization reaction. Indeed, larger variations are observed for β-CDPMA samples compared to the β-CDCDI nanosponges previously investigated[14] in the considered CD/cross-linking agent molar ratio range (specifically, I_4 varies ∼7.4% for β-CDCDI and ∼29.6% for β-CDPMA). This result confirms the regioselectivity of the chemical derivatization of CD during the nanosponge synthesis, involving the primary OH groups mainly.[14]

Also, the behavior of the population I_2, assigned to the secondary OH groups of the native cyclodextrin, as a function of the molar ratio n deserves some comments. I_2 increases with n, and the rate of growth of I_2 is once again higher than the corresponding values determined for β-CDCDI. In detail, I_2

dx.doi.org/10.1021/jp303006a | J. Phys. Chem. B 2012, 116, 7952−7958

Table 1. Main Best-Fit Parameters, i.e., Wavenumbers ω_i (i = 1, 2, 3, 4, and 5) (cm^{-1}), Percentage Intensities I_i (i = 1, 2, 3, 4, and 5) (%), and Vibrational Assignment of the Observed Sub-Bands for the O−H Stretching Region of β-CDPMA Nanosponges at the Analysed β-CD/PMA Molar Ratios

	O−H stretching intersitital H_2O		O−H stretching secondary OH groups		O−H stretching interstitial H_2O		O−H stretching primary OH groups		O−H stretching intracavity H_2O	
T (K)	ω_1 (cm^{-1})	I_1 (%)	ω_2 (cm^{-1})	I_2 (%)	ω_3 (cm^{-1})	I_3 (%)	ω_4 (cm^{-1})	I_4 (%)	ω_5 (cm^{-1})	I_5 (%)
					n = 2					
250	3113.4	6.8	3199.3	15.7	3285.7	21.3	3378.6	36.2	3530.9	20.0
260	3108.4	3.9	3187.6	16.1	3272.8	16.6	3365.4	44.5	3537.8	18.9
270	3108.4	2.9	3186.8	18.1	3272.2	14.1	3362.8	45.0	3534.5	19.9
280	3105.2	2.1	3190.2	20.7	3275.1	12.9	3360.2	45.2	3525.5	19.1
290	3105.2	2.0	3192.5	20.7	3275.4	12.3	3360.2	45.3	3525.5	19.7
300	3108.8	1.5	3198.8	23.1	3274.9	8.5	3361.6	45.9	3535.9	21.0
310	3106.4	1.5	3204.6	26.6	3279.7	7.7	3361.3	46.2	3533.0	18.0
					n = 2.5					
300	3111.5	1.4	3238.8	44.4	3328.7	17.1	3402.1	16.3	3515.1	20.8

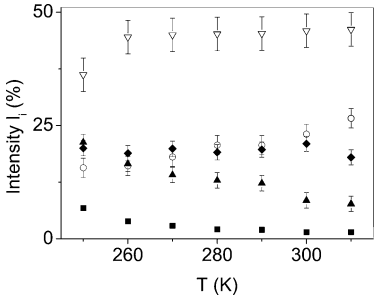

Figure 2. Temperature evolution of the percentage intensities I_i (i = 1, 2, 3, 4, and 5) of the different spectral contributions to the O−H stretching band for β-CDPMA12. I_1, closed squares; I_2, open circles; I_3, closed up triangles; I_4, open down triangles; I_5, closed diamonds.

varies ∼2.2% for β-CDCDI and ∼21.3% for β-CDPMA. In this case, the rationale for the observed trend is less straightforward. A possible explanation relies upon the increased steric hindrance of the whole system with growing cross-linking degree. Distortions of the single cyclodextrin unit from ideal C7 symmetry lead to the disruption of the intramolecular H-bond network at the larger rim of the CD macrocycles.

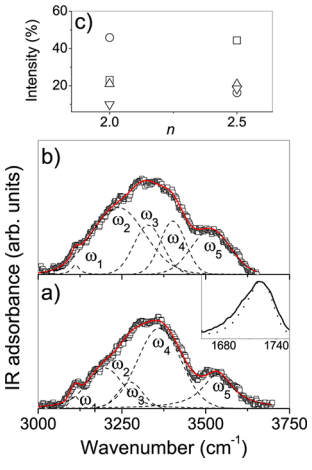

Figure 3. Experimental FTIR-ATR spectra for β-CDPMA12 (a) and β-CDPMA12.5 (b), at T = 300 K, in the OH stretching region together with the best-fit (continuous red line) and the deconvolution components (dashed lines). Inset, experimental profile of the C═O stretching band for β-CDPMA12 (continuous line) and β-CDPMA12.5 (dotted line). Relative intensities for β-CDPMA as a function of β-CD/PMA molar ratio (c); I_1 + I_3, open squares; I_2, open circles; I_4, open up triangles; I_5, open down triangles.

As a final remark, it is worth stressing that the effects on the OH group populations above-discussed are largely dependent on the chemical nature of the cross-linker. As a matter of fact, the carbonate functional group generated by CDI is conformationally more rigid than the ester group formed by condensation of PMA with the OH groups of cyclodextrins, which probably lead to a more flexible structure. This point can be supported by the experimental observation that the CDI−nanosponges are not-swellable, while those obtained with PMA show significant swelling in the presence of water or water solutions.

The analysis of the OH stretching band provides also important information on the redistribution of water among the different hydrogen bonds sites, according to a mechanism suggested by the variations of the populations of interstitial (I_1 + I_3) and intracavity (I_4) H_2O molecules.[29,30] In the case of β-CDPMA nanosponges, by increasing the amount of the cross-linking agent, water molecules are forced to change their environment and rearrange in a new hydrogen bonds scheme, that will be characterized by a major number of interstitial hydrogen-bonded clusters of water molecules (I_1 + I_3 increases of ∼8.5%, while I_5 remains essentially unchanged within the experimental error).

In Figure 4a and 4b, we report, respectively, the FTIR-ATR and Raman spectra collected in the 1500−1800 cm^{-1} wavenumber range for the β-CDPMA12, as an example. In this frequency region of vibrational spectra of nanosponges falls the intense band centered at ∼1722 cm^{-1} in the IR and at ∼1728 cm^{-1} in the Raman spectrum assigned to the carbonyl stretching vibrations of esterified PMA. This band can be conveniently used as a quantitative descriptor of the cross-linking degree of the polymer network.

The high quality of the infrared and Raman spectra of Figure 4 makes their quantitative analysis feasible, by using second derivative computation and curve-fitting procedures with the aim of separating the contribution of the individual spectral components from the broad band observed between 1650 and 1800 cm^{-1}. In order to overcome the problem arising from the partial overlapping with the C═O stretching band of the peaks falling, respectively, at ∼1585 and 1603 cm^{-1} in the FTIR-ATR and Raman spectra and assigned to PMA ring breathing modes, the simultaneous fit of the whole spectra between 1500 and

dx.doi.org/10.1021/jp303006a | J. Phys. Chem. B 2012, 116, 7952−7958

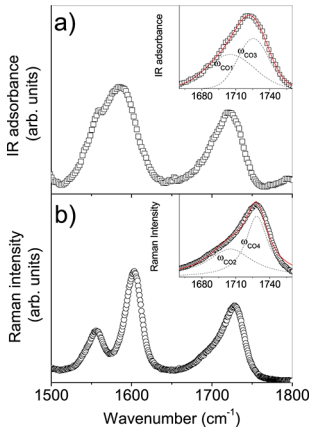

Figure 4. Experimental FTIR-ATR (a) and Raman (b) spectra for β-CDPMA12 in the 1500−1800 cm^{-1} wavenumber range, at room temperature. Inset: fitting results for the C═O stretching band.

1800 cm^{-1} was carried out, with all the fitting parameters left free to vary upon iteration until convergence is reached. Then, the contributions arising from the modes at ∼1585 and 1603 cm^{-1} have been subtracted from the experimental data and more detailed fits have been performed just for the C═O stretching band, both in FTIR-ATR and Raman spectrum (see insets of Figure 4). In this way, four components of the C═O stretching band were extracted, i.e., $\omega_{CO1} \approx 1705$ cm^{-1} (IR active), $\omega_{CO2} \approx 1706$ cm^{-1}(Raman active), $\omega_{CO3} \approx 1726$ cm^{-1} (IR active), and $\omega_{CO4} \approx 1729$ cm^{-1} (Raman active). These components correctly describe the existing types of carbonyl stretching modes assigned, respectively, to the vibrations of the C═O belonging to the ester groups (ω_{CO1} and ω_{CO2}) and to the carboxylic groups (ω_{CO3} and ω_{CO4}) of the bridging molecule.

This assignment is confirmed by the comparison of the theoretical IR and Raman spectra computed on the model shown in Figure 5 and the experimental vibrational spectra of

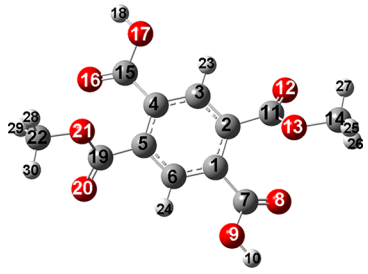

Figure 5. Model of the simulated bridging molecule; the labeling of the atoms is the one adopted for the ab initio computation.

β-CDPMA12 nanosponge in the wavenumber range 1670−1760 cm^{-1}, where cyclodextrins do not show any interfering vibrational band (Figure 6).

The model shown in Figure 5 mimics the molecular environment of PMA after the reaction with the OH groups of cyclodextrins to form two ester groups (C(11)═O(12) and C(19)═O(20) in Figure 5) and generating two free carboxylic groups (C(7)═O(8) and C(15)═O(16) in Figure 5). This model was built assuming that a maximum of two carbonyl groups of PMA can simultaneously be engaged to form ester linkages with CD molecules.

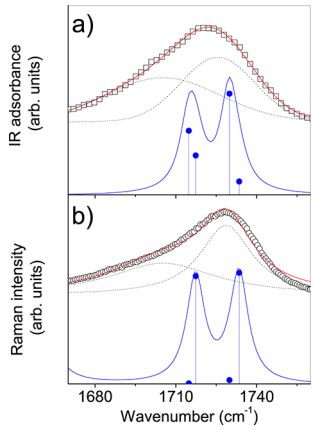

Figure 6. Experimental FTIR-ATR (a) and Raman (b) spectra for β-CDPMA12 (empty symbols) compared with the computed IR (a) and Raman (b) spectrum (continuous line) of linking group in the wavenumber range 1670−1760 cm^{-1}.

On the basis of the wavenumber and relative intensities of the computed peaks, the experimental IR-active spectral components $\omega_{CO1} \approx 1705$ cm^{-1} and $\omega_{CO3} \approx 1726$ cm^{-1} can be associated to the computed peaks at 1715 and 1730 cm^{-1} (Figure 6a). These modes are mainly localized on atoms 11−12, 19−20 (corresponding to the ester groups of bridging molecule), and 7−10, 15−18 (corresponding to the carboxylic groups), respectively. This conclusion can be inferred by inspection of the eigenvector corresponding to the modes at 1715 and 1730 cm^{-1}, which are shown in Figure 7a and 7c.

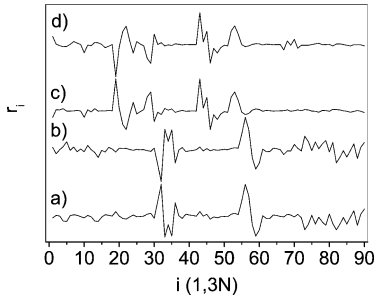

Figure 7. Normalized displacements r_i as a function of the atomic degree of freedom i for each atom of bridging group under the effect of the normal modes at 1715 cm^{-1} (a), 1717 cm^{-1} (b), 1730 cm^{-1} (c), and 1734 cm^{-1} (d).

Here, we report the normalized displacements r_i (i = 1, 3N where N is the number of PMA atoms, labeled in Figure 5) of each PMA atom under the effect of the normal mode obtained at 1715 and 1730 cm^{-1}. Using this representation of the eigenvectors, we can visualize the Cartesian displacements $r_1 = X_1$, $r_2 = Y_1$, $r_3 = Z_1$, $r_4 = X_2$,... for each atom, due to the action of the corresponding normal mode.

Similarly, the experimental Raman-active modes $\omega_{CO2} \approx 1706$ cm^{-1} and $\omega_{CO4} \approx 1729$ cm^{-1} can be associated to the computed modes at 1717 and 1734 cm^{-1} (Figure 6b), corresponding to stretching vibrations of the C═O belonging to the ester groups (Figure 7b) and to the carboxylic groups (Figure 7d) of the PMA residues, respectively.

According to the deconvolution done in the 1600−1800 cm^{-1} region, CDs do not contribute to the C═O stretching signal in the vibrational spectra of nanosponges. Thus, the

dx.doi.org/10.1021/jp303006a | J. Phys. Chem. B 2012, 116, 7952−7958

1600−1800 cm^{-1} region contains the vibrational modes of ester carbonyl and carboxylic groups of PMA only, previously indicated by ω_{CO1} and ω_{CO3} in the FTIR-ATR spectrum and ω_{CO2} and ω_{CO4} in the Raman spectrum.

The total estimated intensity for the C═O stretching band is reported as a function of the β-CD/PMA molar ratio for IR and Raman spectra in Figure 8a and 8b, respectively. The total

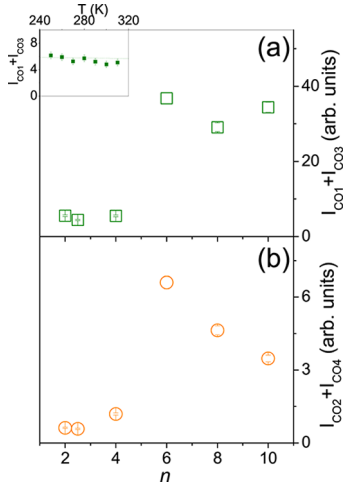

Figure 8. Total intensity estimated for the C═O stretching band observed in FTIR-ATR (a) and Raman (b) spectra as a function of β-CD/PMA molar ratio. Inset: temperature evolution of the total intensity of the C═O stretching band observed in FTIR-ATR spectrum of β-CDPMA12.

estimated intensity is obtained as the sum of the intensities of the two different spectral components (I_{CO1} and I_{CO3} for IR and I_{CO2} and I_{CO4} for Raman data) in which the C═O stretching band has been deconvoluted by using fitting procedure.

In order to allow a quantitative analysis, the spectra were preliminarily normalized to the intensity of the bands at ∼1030 and 2917 cm^{-1} for IR and Raman data, respectively. The latter vibrational modes were assumed to be a reliable internal standard being related to stretching vibrations of C−O and CH_2 groups of cyclodextrin molecules, which are not involved in the reaction of polymerization with PMA.

The normalized intensity of C═O stretching band reflects the population of the corresponding species, in turn, directly proportional to the degree of cross-linking of the nanosponges network. As it can be observed in Figure 8, the plot shows a maximum corresponding to the β-CD/PMA molar ratio = 1:6, whereas for high molar ratios, i.e., >6, the reticulation in cyclodextrin nanosponges seems to decrease, probably for the action of steric effects that prevent further cross-linking of the polymer. This trend seems to indicate that beyond a 6-fold excess of PMA with respect to β-CD, PMA provides branching of cyclodextrin units rather than a further increase of the cross-linking of the whole system. This conclusion is also supported by some low-frequency Raman and Brillouin scattering experiments recently published.[33] In those experiments, the observed shifts of the frequency position of Boson and Brillouin peaks are directly connected to the stiffness of the system over a length scale ranging from a few to hundreds of nanometers. The frequency position of the Boson and Brillouin peaks is a function of n and shows the maximum effect for the β-CD/PMA molar ratio = 1:6,[33] in agreement with the behavior found for C═O stretching band intensity.

A good agreement is also found between IR and Raman results summarized in Figure 8, confirming the reliability of the data treatment and normalization procedure.

The temperature evolution of the total intensity of the C═O stretching band observed in the FTIR-ATR spectrum for β-CDPMA12 is shown in the inset of Figure 8a, as an example. As expected, the intensity of the C═O stretching band in the explored temperature range remains unchanged within the experimental error.

Further important information about the structure of the nanosponges network can be obtained by following the evolution of the intensity of the single spectral components I_{CO} of the C═O stretching band in the vibrational spectra of nanosponges as a function of β-CD/PMA molar ratio.

In Figure 9a and 9b, the percentage intensities (defined as $I_1(\%) = (I_1/(I_1 + I_3))$, $I_2(\%) = (I_2/(I_2 + I_4))$, etc.) of the single

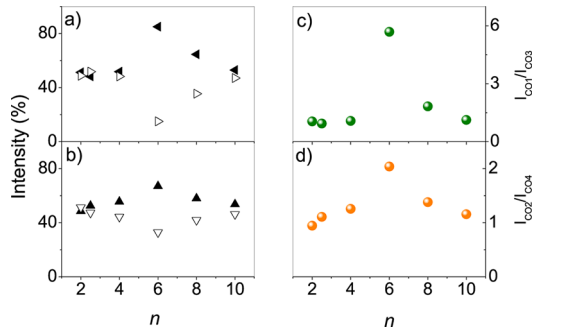

Figure 9. Percentage intensities of the different spectral contributions to the C═O stretching band observed in FTIR-ATR (a) and Raman (b) spectra as a function of β-CD/PMA molar ratio. I_{CO1}, closed left triangle; I_{CO3}, open right triangle; I_{CO2}, closed up triangle; I_{CO4}, open down triangle. Ratio between the intensity of the spectral contributions to the C═O stretching band observed in FTIR-ATR (c) and Raman (d) spectra as a function of n.

spectral components are plotted as a function of n for IR and Raman spectra, respectively.

The form of the eigenvectors corresponding to the normal modes identified with the experimental ω_{CO} components indicates that the type of vibration for the two types of carbonyls found in the PMA moiety is the same, namely, C═O stretching. Thus, we can reasonably assume that the observed percentage intensity I_{CO} is directly proportional to the number of corresponding types of oscillators, i.e., to the amount of the two type of carbonyls present in PMA (I_{CO1} and I_{CO3} for C═O of ester groups; I_{CO2} and I_{CO4} for C═O of carboxylic groups). The excess of ester bonds with respect to the free carboxylic groups is maximum for n = 6, as can be observed by both IR and Raman data of Figure 9a and 9b, respectively. The 6-fold excess of cross-linker with respect to β-CD leads to a saturation effect for the three-dimendional growth of the polymer.

Figure 9c and 9d shows the ratio between the intensities of the spectral components I_{CO1}/I_{CO3} and I_{CO2}/I_{CO4} as a function of n, respectively. These quantities reflect the ratio between the populations of ester and carboxylic groups estimated by IR and Raman data. Also, in this case, the results are coherent and confirm the reliability of the IR−Raman approach here proposed.

dx.doi.org/10.1021/jp303006a | J. Phys. Chem. B 2012, 116, 7952−7958

CONCLUSIONS

In this article, we report on the results of a multitechnique study of a new class of nanostructured soft materials, obtained by polymerization of cyclodextrins into a 3-dimensional network. Important information on the molecular structure of these innovative systems are provided by the combined use of Raman and infrared spectroscopy, also supported by quantum chemical calculations.

By focusing on the frequency range between 1500 and 1800 cm^{-1}, where the C═O stretching modes of the system fall, we conclude that the degree of cross-linking of the polymeric network can be effectively tuned by varying the molar ratio between the cross-linking agent PMA and the monomer β-CD, leading to a final product with different stiffness. More interestingly, by monitoring the IR and Raman intensity evolution of the spectral components assigned to the stretching vibrations of carboxylic and ester C═O groups, we observe a maximum in the cross-linking of the network, corresponding to 6-fold excess of cross-linker with respect to β-CD; this value of CD/PMA molar ratio also coincides with the saturation of all the reactive sites of cross-linker, probably due to steric hindrance affects. Finally, the detailed inspection of the high frequency vibrational dynamics of nanosponges reveled a clear dependence from temperature and from PMA/CD molar ratio of the H-bond network involving the OH groups of the molecule.

This experimental and numerical approach, here successfully applied to a model class of nanoporous polymers, appears very promising for the structural investigation of other amorphous polymers for which the use of X-ray diffraction techniques is seriously hampered by the low or absent level of crystallinity.

AUTHOR INFORMATION

Corresponding Author

*E-mail: rossi@science.unitn.it.

Notes

The authors declare no competing financial interest.

ACKNOWLEDGMENTS

We would like to thank Dr. A. Defant for useful discussions. B.R. acknowledges the financial support of the Regione Veneto, being the beneficiary of a scholarship within the Programma Operativo Regionale FSE 2007-2013.

REFERENCES

(1) Trotta, F.; Tumiatti, W. Cross-Linked Polymers Based on Cyclodextrin for Removing Polluting Agents. Patent WO 03/085002, 2003.

(2) Trotta, F.; Tumiatti, W.; Cavalli, R.; Zerbinati, O.; Roggero, C. M.; Vallero, R. Ultrasound-Assisted Synthesis of Cyclodextrin-Based Nanosponges. Patent WO 06/002814, 2006.

(3) Cavalli, R.; Trotta, F.; Tumiatti, W. *J. Inclusion Phenom. Macrocyclic Chem.* **2006**, *56*, 209.

(4) Trotta, F.; Cavalli, R. *Compos. Interfaces* **2009**, *16*, 39.

(5) Swaminathan, S.; Vavia, P. R.; Trotta, F.; Torne, S. *J. Inclusion Phenom. Macrocyclic Chem.* **2007**, *57*, 89.

(6) Swaminathan, S.; Pastero, L.; Serpe, L.; Trotta, F.; Vavia, P. R.; Aquilano, D.; Trotta, M.; Zara, G.; Cavalli, R. *Eur. J. Pharm. Biopharm.* **2010**, *74*, 193.

(7) Ansari, K. A.; Vavia, P. R.; Trotta, F.; Cavalli, R. *AAPS PharmSciTech* **2011**, *12*, 279.

(8) Seglie, L.; Martina, K.; Devecchi, M.; Roggero, C.; Trotta, F.; Scariot, V. *Postharvest Biol. Technol.* **2011**, *59*, 200.

(9) Trotta, F.; Tumiatti, W.; Cavalli, R.; Roggero, C. M.; Mognetti, B.; Berta Nicolao, G. Cyclodextrin-Based Nanosponges As a Vehicle for Antitumoral Drugs. Patent WO 09/003656, 2009.

(10) Vyas, A.; Shailendra, S.; Swarnlata, S. *J. Inclusion Phenom. Macrocyclic Chem.* **2008**, *62*, 23.

(11) Mamba, B. B.; Krause, R. W.; Malefetse, T. J.; Gericke, G.; Sithole, S. P. *Water SA* **2008**, *34*, 657.

(12) Arkas, M.; Allabashi, R.; Tsiourvas, D.; Mattausch, E. M.; Perfler, R. *Environ. Sci. Technol.* **2006**, *40*, 2771.

(13) Mele, A.; Castiglione, F.; Malpezzi, L.; Ganazzoli, F.; Raffaini, G.; Trotta, F.; Rossi, B.; Fontana, A.; Giunchi, G. *J. Inclusion Phenom. Macrocyclic Chem.* **2011**, *69*, 403.

(14) Castiglione, F.; Crupi, V.; Majolino, D.; Mele, A.; Panzeri, W.; Rossi, B.; Trotta, F.; Venuti, V. *J. Inclusion Phenom. Macrocyclic Chem.* **2012**, DOI: 10.1007/s10847-012-0106-z.

(15) Maréchal, Y. *J. Mol. Struct.* **2003**, *648*, 27.

(16) Lewiner, L.; Klein, J. P.; Puel, F.; Fevotte, G. *Chem. Eng. Sci.* **2001**, *56*, 2059.

(17) Hahn, B. D.; Neubert, R. H. H.; Wartewig, S.; Christ, A.; Hentzsch, C. *J. Pharm. Sci.* **2000**, *89*, 1106.

(18) Gajewski, J. J.; Gilbert, K. E. *PCModel 8.0*, molecular modelling software for personal workstation; Serena Software: Bloomington, IN, 2002.

(19) Frisch, M. J.; Trucks, G. W.; Schlegel, H. B.; Scuseria, G. E.; Robb, M. A.; Cheeseman, J. R.; Montgomery, J. A., Jr.; Vreven, T.; Kudin, K. N.; Burant, J. C.; Millam, J. M.; Iyengar, S. S.; Tomasi, J.; Barone, V.; Mennucci, B.; Cossi, M.; Scalmani, G.; Rega, N.; Petersson, G. A.; Nakatsuji, H.; Hada, M.; Ehara, M.; Toyota, K.; Fukuda, R.; Hasegawa, J.; Ishida, M.; Nakajima, T.; Honda, Y.; Kitao, O.; Nakai, H.; Klene, M.; Li, X.; Knox, J. E.; Hratchian, H. P.; Cross, J. B.; Bakken, V.; Adamo, C.; Jaramillo, J.; Gomperts, R.; Stratmann, R. E.; Yazyev, O.; Austin, A. J.; Cammi, R.; Pomelli, C.; Ochterski, J. W.; Ayala, P. Y.; Morokuma, K.; Voth, G. A.; Salvador, P.; Dannenberg, J. J.; Zakrzewski, V. G.; Dapprich, S.; Daniels, A. D.; Strain, M. C.; Farkas, O.; Malick, D. K.; Rabuck, A. D.; Raghavachari, K.; Foresman, J. B.; Ortiz, J. V.; Cui, Q.; Baboul, A. G.; Clifford, S.; Cioslowski, J.; Stefanov, B. B.; Liu, G.; Liashenko, A.; Piskorz, P.; Komaromi, I.; Martin, R. L.; Fox, D. J.; Keith, T.; Al-Laham, M. A.; Peng, C. Y.; Nanayakkara, A.; Challacombe, M.; Gill, P. M. W.; Johnson, B.; Chen, W.; Wong, M. W.; Gonzalez, C.; Pople, J. A. *Gaussian 03*, revision C.02; Gaussian, Inc.: Wallingford, CT, 2003.

(20) Lee, C.; Yang, W.; Parr, R. G. *Phys. Rev. B* **1988**, *37*, 785.

(21) Becke, A. D. *J. Chem. Phys.* **1993**, *98*, 5648.

(22) Hariharan, P. C.; Pople, J. A. *Theor. Chim. Acta* **1973**, *28*, 213.

(23) Crupi, V.; Longo, F.; Majolino, D.; Venuti, V. *J. Phys.: Condens. Matter* **2006**, *18*, 3563.

(24) Crupi, V.; Longo, F.; Majolino, D.; Venuti, V. *J. Chem. Phys.* **2005**, *123*, 154702.

(25) Mallamace, F.; Broccio, M.; Corsaro, C.; Faraone, A.; Majolino, D.; Venuti, V.; Liu, L.; Mou, C. Y.; Chen, S. H. *Proc. Natl. Acad. Sci. U.S.A.* **2007**, *104*, 424.

(26) Crupi, V.; Ficarra, R.; Guardo, M.; Majolino, D.; Stancanelli, R.; Venuti, V. *J. Pharm. Biomed. Anal.* **2007**, *44*, 110.

(27) Cannavà, C.; Crupi, V.; Ficarra, P.; Guardo, M.; Majolino, D.; Stancanelli, R.; Venuti, V. *Vib. Spectrosc.* **2008**, *48*, 172.

(28) Stancanelli, R.; Ficarra, R.; Cannavà, C.; Guardo, M.; Calabrò, M. L.; Ficarra, P.; Ottanà, R.; Maccari, R.; Crupi, V.; Majolino, D.; Venuti, V. *J. Pharm. Biomed. Anal.* **2008**, *47*, 704.

(29) Gavira, J. M.; Hernanz, A.; Bratu, I. *Vib. Spectrosc.* **2003**, *32*, 137.

(30) Bratu, I.; Veiga, F.; Fernandes, C.; Hernanz, A.; Gavira, J. M. *Spectroscopy* **2004**, *18*, 459.

(31) Rey, R.; Møller, K. B.; Hynes, J. T. *J. Phys. Chem. A* **2002**, *106*, 11993.

(32) Møller, K. B.; Rey, R.; Hynes, J. T. *J. Phys. Chem. A* **2004**, *108*, 1275.

(33) Rossi, B.; Caponi, S.; Castiglione, F.; Corezzi, S.; Fontana, A.; Giarola, M.; Mariotto, G.; Mele, A.; Petrillo, C.; Trotta, F.; Viliani, G. *J. Phys. Chem. B* **2012**, *116* (17), 5323.